Received: 17 September 2023 | Revised: 2 November 2023 | Accepted: 11 November 2023

DOI: 10.1002/jcc.27266

RESEARCH ARTICLE

Journal of COMPUTATIONAL CHEMISTRY WILEY

MARVEL analysis of high-resolution rovibrational spectra of $^{13}C^{16}O_2$

Mohammad Taha I. Ibrahim [1,2] | Dunia Alatoom [1,2] | Tibor Furtenbacher [3] | Attila G. Császár [4] | Sergei N. Yurchenko [2] | Ala'a A. A. Azzam [1,5] | Jonathan Tennyson [2]

[1]AstroJo Institute, Amman, Jordan

[2]Department of Physics and Astronomy, University College London, London, UK

[3]HUN-REN–ELTE Complex Chemical Systems Research Group, Budapest, Hungary

[4]ELTE Eötvös Loránd University, Institute of Chemistry, Budapest and HUN-REN–ELTE Complex Chemical Systems Research Group, Budapest, Hungary

[5]Department of Physics, The University of Jordan, Amman, Jordan

Correspondence
Attila G. Császár, ELTE Eötvös Loránd University, Institute of Chemistry, Pázmány Péter sétány 1/A and HUN-REN–ELTE Complex Chemical Systems Research Group, H-1117, H-1532 Budapest, P.O. Box 32, Hungary.
Email: attila.csaszar@ttk.elte.hu

Jonathan Tennyson, Department of Physics and Astronomy, University College London, London, UK.
Email: j.tennyson@ucl.ac.uk

Funding information
European Cooperation in Science and Technology; European Research Council; Nemzeti Kutatási Fejlesztési és Innovációs Hivatal; Science and Technology Facilities Council

Abstract

A set of empirical rovibrational energy levels, obtained through the MARVEL (measured active rotational-vibrational energy levels) procedure, is presented for the $^{13}C^{16}O_2$ isotopologue of carbon dioxide. This procedure begins with the collection and analysis of experimental rovibrational transitions from the literature, allowing for a comprehensive review of the literature on the high-resolution spectroscopy of $^{13}C^{16}O_2$, which is also presented. A total of 60 sources out of more than 750 checked provided 14,101 uniquely measured and assigned rovibrational transitions in the wavenumber range of 579–13,735 cm^{-1}. This is followed by a weighted least-squares refinement yielding the energy levels of the states involved in the measured transitions. Altogether 6318 empirical rovibrational energies have been determined for $^{13}C^{16}O_2$. Finally, estimates have been given for the uncertainties of the empirical energies, based on the experimental uncertainties of the transitions. The detailed analysis of the lines and the spectroscopic network built from them, as well as the uncertainty estimates, all serve to pinpoint possible errors in the experimental data, such as typos, misassignment of quantum numbers, and misidentifications. Errors found in the literature data were corrected before including them in the final MARVEL dataset and analysis.

KEYWORDS
CO_2, line positions, MARVEL, rovibrational energy levels

1 | INTRODUCTION

Carbon dioxide is a well-known trace species in the Earth's atmosphere, the recent increase in its concentration is associated with human activity, and it is involved in climate change.[1] Most of the spectral regions corresponding to the main isotopologue, $^{12}C^{16}O_2$, are optically thick, meaning that increases in atmospheric concentration lead only to logarithmic increase in the radiative forcing associated with the so-called greenhouse effect (see, e.g., Reference 2). In the atmosphere of Earth, about 1.1% of CO_2 is in the form of the $^{13}C^{16}O_2$ isotopologue.[3] The corresponding spectral lines are not optically thick, increasing the importance of this isotopologue as a greenhouse gas.

While ^{13}C is only a minor constituent in the Earth's atmosphere, the ^{13}C to ^{12}C abundance ratio is known to vary significantly in the Universe. There are observations which suggest that at places

the ratio might be as high as one third.[4] The detection of CO_2 in the atmospheres of hot Jupiter exoplanets,[5] including a recent one on WASP-39b by the James Webb Space Telescope,[6] have all been made using low- to medium-resolution transit spectroscopy, which cannot distinguish between different isotopologues. Thus, these observations are unable to provide information on isotopic ratios. However, high-resolution, cross-correlation studies performed from the ground have been shown to be capable of distinguishing different carbon isotopologues; for example, a pioneering study of CO of exoplanet TYC 8998-760-1 b suggested that the abundance of ^{13}C was more than 30 % of that of ^{12}C.[7]

High-resolution studies of exoplanet spectra require especially accurate line positions. There are line lists available for hot CO_2,[8–11] but these are generally not of sufficient accuracy for use in cross-correlation studies for high-temperature objects. The most practical means of improving the accuracy of theoretical line lists is the introduction of experimental/empirical energy-level data, facilitating the development of improved line positions. Supplying empirical rovibrational energy levels for $^{13}C^{16}O_2$ was one of the motivations of the present project.

The MARVEL (measured active rotational-vibrational energy levels)[12–15] procedure, based on the theory of spectroscopic networks (SN),[16–18] is able to provide such highly accurate empirical energy levels. For this, we need a dataset of experimental line positions, which we created for the carbon dioxide isotopologue $^{16}O^{13}C^{16}O$ (636 in HITRAN parlance). MARVEL determines the SN representing all interconnecting rotational-vibrational energy levels and, based on an inversion process, yields empirical energy levels with appropriate uncertainties. Besides providing these data, a MARVEL analysis is able to identify incorrect quantum number assignments, overly optimistic uncertainty values, mistaken attributions, and many other types of errors. The empirical rovibrational energies can be used to check and improve existing theoretical models, as well as line lists, for example those generated within the ExoMol project.[19,20] The joint utilization of the best empirical and theoretical data provides both completeness and the most accurate predictions of transition frequencies, see References 21 and 22 for examples. Our critical evaluation of the existing empirical line positions also helps to identify spectral regions where more high-resolution experiments are needed.

2 | COMPUTATIONAL BACKGROUND

2.1 | The MARVEL procedure

A MARVEL project begins by gathering, analyzing, and validating assigned lines of high-resolution spectra. Attributes of each line, besides their position, include a unique label for the upper and lower states, a measurement uncertainty value, and a unique tag identifier. The lines are then used to build a spectroscopic network, whereby each state corresponds to a node, and the nodes are linked by the observed transitions.[16] This representation of the spectroscopic measurement results allows the determination of empirical energy-level values, together with their uncertainty estimates. The transitions form a well-connected network, with most transitions linked to the ground state *via* various paths. However, this connection is not always possible using experimental data alone. The missing lines may result in fragmentation of the principal component(s) of the SN. As a result, consistency of the lines of the floating components with the rest of the data cannot be established. This is the reason why such lines remain unvalidated at the end of a MARVEL analysis.

Since MARVEL is not based on a particular quantum-chemical model, it will "validate" forbidden or incorrect transitions when they are not in conflict with the rest of the data. For this reason, it is important to check for such transitions while building up the MARVEL input dataset.

2.2 | Quantum numbers and selection rules

There are two conventions in general use for assigning quantum numbers to the vibrational states of the linear molecule CO_2. The standard, so-called Herzberg notation is based on the harmonic oscillator (HO) picture and uses four vibrational quantum numbers, $(\tilde{\nu}_1, \tilde{\nu}_2^{\tilde{\ell}_2}, \tilde{\nu}_3)$, where $\tilde{\nu}_1$, $\tilde{\nu}_2$, and $\tilde{\nu}_3$ describe the symmetric stretch, bend, and antisymmetric stretch of the molecule, respectively, while $\tilde{\ell}_2$ denotes the angular momentum associated with the bending mode and can take values of $\tilde{\nu}_2$, $\tilde{\nu}_2 - 2$, $\tilde{\nu}_2 - 4$, ..., 1 or 0. Complications induced by the well-known Fermi resonance between the ν_1 and $2\nu_2$ states of CO_2 led to the introduction of the so-called AFGL (air force geophysics laboratory) notation,[3,23,24] which is adopted here. The AFGL notation groups the vibrational states into Fermi polyads and uses five vibrational quantum numbers, $(v_1\ v_2\ \ell_2\ v_3\ r)$, where r is the Fermi-resonance ranking index. In this notation, the Fermi polyads are determined by v_1, ℓ_2, and v_3;[25] v_2 is always equal to ℓ_2, and r takes values from 1 to v_1+1. To the best of our knowledge, there is no unambiguous conversion between the Herzberg and the AFGL conventions; hence, we used data from multiple datasets to match the Herzberg notation to AFGL. Since the first release of the HITRAN database,[23] it has been emphasized that when using older notations the order of some energy levels can change from one CO_2 isotopologue to the other, as shown by the work of Amat and Pimbert.[26]

In addition to the vibrational quantum numbers, there are two further quantum numbers required to label the rovibrational states of CO_2: quantum number J, describing the overall rotation of the molecule, which takes values of $J \geq \ell_2$, and parity, p, for which we use the rotationless parity denoted by e and f.[27] Unlike the vibrational quantum numbers, J and p are rigorously conserved (they are exact quantum numbers). For our MARVEL procedure we employ the AFGL notation and each rovibrational state has the label $(J\ \ v_1\ v_2\ \ell_2\ v_3\ r\ p)$. States with $\ell_2 = 0$ all have parity e. In principle, states with $\ell_2 > 0$ can be both e and f, but due to the Pauli principle, half the rotational levels are missing; to be present, $(J + v_3 + \ell_2 + p)$, where $p = 0$ for e and 1 for f states, must be even.

It is standard to use the point group $D_{\infty h}$ labels to denote levels. In this notation $\Sigma, \Pi, \Delta, \ldots$ represent $\ell_2 = 0, 1, 2, \ldots$, and the other symmetry labels are included as:

$$(-1)^{J+p} = \begin{cases} 1 \rightarrow & \Sigma^+ \\ -1 \rightarrow & \Sigma^- \end{cases} \quad (1)$$

$$(-1)^{(v_3+\ell_2)} = \begin{cases} 1 \rightarrow & g \\ -1 \rightarrow & u \end{cases} \quad (2)$$

When building up the MARVEL input file, we tested for incorrectly labelled transitions in the dataset to ensure the correctness of all the lines. As part of this procedure, obeyance of dipole selection rules were checked. For the $^{13}C^{16}O_2$ isotopologue, they include vibrational,

$$(-1)^{(\Delta v_2+\Delta v_3)} = -1, \quad (3)$$

rovibrational,

$$\Sigma_g^+ \leftrightarrow \Sigma_u^-, \quad (4)$$

and rotational,

$$\Delta J = -1, 0, +1, \quad (5)$$

$$\text{if } \Delta J = \pm 1, \text{then e} \leftrightarrow \text{e, f} \leftrightarrow \text{f,}$$

$$\text{if } \Delta J = 0, \text{then e} \leftrightarrow \text{f but } J = 0 \not\leftrightarrow 0,$$

selection rules.[25] These selection rules, as well as the Pauli-principle constraint, were all used to verify the labels of the experimental transitions obtained from the literature.

2.3 | Resonances in CO_2

Various types of resonances affect the infrared spectra of carbon dioxide, such as Fermi, Coriolis, and ℓ-type resonances.[25,28] These resonance effects complicate the energy-level labeling due to occurrences of overlapping transitions, contributing to the complexity of the spectral patterns. Figure 1 shows the considerable effects Fermi-type resonances have on the experimental spectrum.

The MARVEL procedure is able to find discrepancies in the energy-level labels and can find transitions misassigned due to various types of resonances. Nevertheless, a comparison with the assignments present in the NASA Ames-2021 variational line list[29] and the effective Hamiltonian Carbon Dioxide Spectroscopic Databank (CDSD) line list[30] was performed. In accordance with recent studies that analyzed some of these effects,[31,32] our study verifies many of the reassignments made. We also make further reassignments, not suggested previously (*vide infra*).

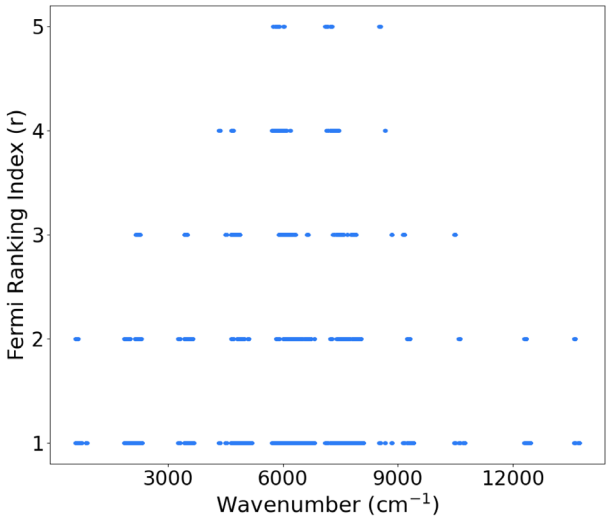

FIGURE 1 Distribution of the Fermi ranking index, *r*, across the experimental spectral region covered, illustrating the overlapping of transitions.

2.4 | Beat frequencies

Some of the states of CO_2 have been the subject of a series of high-accuracy measurements of beat frequencies.[33–44] A beat frequency is the result of mixing two frequencies. This kind of measurement is often made using the heterodyne measurement technique, which gives very accurate results. However, unlike absolute frequencies, which form the input of the standard MARVEL procedure, beat frequencies do not correspond to a specific line position and a pair of lower and upper states. Beat-frequency measurements connect four energy levels using just one frequency, which represents the difference between two transition frequencies. In an absolute frequency measurement, the frequency (ν) represents the difference between two energy levels, $\nu \propto E_2 - E_1$. For a beat-frequency measurement, the frequency (ν_b) corresponds to the difference between four energy levels, $\nu_b \propto (E_2 - E_1) - (E_4 - E_3)$.

Beat-frequency measurements cannot be used with the standard MARVEL algorithm.[13–15,45] Initial tests, which included beat frequencies as extra data in the MARVEL process, were found to lead to ill-conditioned matrices even when the four levels involved in the measured beats were well determined by the standard SN. Ill-conditioning occurs when the beat-frequency measurements have a lower uncertainty than the standard measurements determining the energy levels involved. Of course, this is precisely the case when beat-frequency data are of real interest.

3 | METHODOLOGY

3.1 | Data collection

The present study started by collecting and analyzing literature sources that discuss high-resolution rovibrational spectra of carbon dioxide. More than 750 sources were analyzed and given a tag, using

TABLE 1 Experimental sources of $^{13}C^{16}O_2$ rovibrational transitions, the wavenumber range they span, numbers of lines, uncertaintity information and the labelling scheme used in each source.

Source	Range / cm^{-1}	A/V[a]	*CSU*[b]	*MSU*[c]	Notation
85Jolma[62]	579–759	507/507	5.00×10^{-4}	5.46×10^{-4}	Other
80PaKaAn[63]	598–694	79/79	1.18×10^{-3}	1.90×10^{-3}	Other
01Miller[64]	613–6796	611/611	2.16×10^{-4}	8.47×10^{-4}	Other
83JoKaHo[65]	613–685	68/68	4.50×10^{-3}	4.50×10^{-3}	Other
86GuRa[66]	619–2281	75/75	5.00×10^{-4}	5.04×10^{-4}	Other
78ReFl[67]	648–649	14/14	1.00×10^{-3}	2.26×10^{-3}	Other
81PeWeMaSi[44]	849–907	31/31	2.07×10^{-3}	2.07×10^{-3}	Other
84RiBeDeFe[68]	1852–2099	335/334	1.01×10^{-3}	1.69×10^{-3}	AFGL
85RiBeDe[69]	1859–1996	55/55	1.00×10^{-3}	1.17×10^{-3}	AFGL
84RiBe[70]	1983–2092	106/106	1.00×10^{-3}	1.38×10^{-3}	AFGL
12LyKaJaLu[71]	1996–6263	383/383	1.00×10^{-3}	1.31×10^{-3}	AFGL
86RiBeDe[72]	2056–2182	79/79	1.00×10^{-3}	1.16×10^{-3}	AFGL
82EsHuSaVa[24]	2142–2333	674/662	6.00×10^{-4}	7.75×10^{-4}	AFGL
86EsSaRoVa[73]	2142–2309	562/515	8.26×10^{-4}	1.12×10^{-3}	AFGL
86EsRo[74]	2143–2296	340/291	8.03×10^{-4}	1.04×10^{-3}	AFGL
83EsRo[75]	2150–2333	237/236	6.91×10^{-4}	1.01×10^{-3}	AFGL
77StToCl[54]	2077–2324	834/834	1.00×10^{-3}	1.29×10^{-3}	Other
78DeBaGrLi[76]	2173–2329	91/91	1.50×10^{-3}	2.18×10^{-3}	Other
78BaLiDeRa[56]	2179–2315	679/675	3.00×10^{-3}	3.56×10^{-3}	Other
84BaRo[77]	2192–2322	198/198	1.00×10^{-4}	2.08×10^{-4}	Other
15ElSuMi[78]	2214–2323	60/60	3.00×10^{-6}	3.00×10^{-6}	AFGL
68ObRaHaMcO[53]	2214–2319	144/144	1.15×10^{-2}	1.78×10^{-2}	Other
68ObRaHaMcP[53]	2228–2320	140/139	1.20×10^{-2}	1.45×10^{-2}	Other
67Hahn[52]	2228–2314	126/125	4.25×10^{-3}	8.09×10^{-3}	Other
80Guelachvili[79]	2235–2315	117/117	1.58×10^{-4}	3.36×10^{-4}	Other
88BeDeRiFe[80]	3246–3330	31/31	1.00×10^{-3}	1.88×10^{-3}	AFGL
82BaRiSmRa[57]	3420–3681	1224/1224	5.00×10^{-3}	4.80×10^{-3}	Other
14BoJaLyTa[81]	3460–3665	210/210	1.09×10^{-4}	1.95×10^{-4}	AFGL
55FrDl[82]	3592–3662	47/46	1.34×10^{-2}	8.17×10^{-2}	Other
65GoRo[61]	3600–3663	30/30	5.00×10^{-3}	6.96×10^{-3}	Other
16VaKoMoKa[83]	4315–4374	10/10	2.00×10^{-3}	2.61×10^{-3}	AFGL
05GaLiCeCa[84]	4321–4364	9/9	2.00×10^{-3}	3.05×10^{-3}	AFGL
22MaBoPeSo[85]	4488–4549	20/20	3.20×10^{-4}	4.66×10^{-4}	AFGL
04DiMaRoPe[59]	4636–8104	4444/4417	1.00×10^{-3}	1.68×10^{-3}	AFGL
16BeDeSuBr[60]	4695–4932	430/429	1.39×10^{-3}	1.76×10^{-3}	AFGL
08PeDeLiKa[31]	4703–6796	1114/1112	2.00×10^{-4}	5.54×10^{-4}	AFGL
15BoJaLyTa[86]	4728–5019	99/99	2.37×10^{-4}	4.80×10^{-4}	AFGL
49GoMoMcPi[87]	4728–4910	48/47	1.00×10^{-2}	5.82×10^{-2}	Other
12ChSpMeJa[88]	4866–4880	9/9	4.00×10^{-4}	8.42×10^{-4}	AFGL
18KaSiCeMo[89]	5702–5851	233/233	1.00×10^{-3}	1.10×10^{-3}	AFGL
18CeKaMoKa[90]	5733–5877	68/68	1.00×10^{-3}	1.18×10^{-3}	AFGL
08PePeCa[32]	5892–6837	489/489	1.05×10^{-3}	1.57×10^{-3}	AFGL
06PeKaRoPe[91]	5957–6796	761/761	1.00×10^{-3}	1.25×10^{-3}	AFGL
16DeBeSuBr[92]	6078–6271	102/102	2.40×10^{-4}	4.16×10^{-4}	AFGL
07PeKaRoPe[93]	6130–6668	484/484	2.00×10^{-3}	2.26×10^{-3}	AFGL

TABLE 1 (Continued)

Source	Range / cm^{-1}	A/V[a]	CSU[b]	MSU[c]	Notation
23LiCaZhHu[94]	6270	1/1	1.50×10^{-6}	1.50×10^{-6}	AFGL
10CaSoMoPe[95]	7078–7916	2183/2183	6.29×10^{-4}	8.30×10^{-4}	AFGL
09KaSoCa[96]	7147–7774	318/318	5.00×10^{-4}	9.64×10^{-4}	AFGL
10SoKaTaPe[97]	7147–7916	369/369	1.00×10^{-3}	1.35×10^{-3}	AFGL
17KaKaTaPe[98]	7296–7916	159/159	1.00×10^{-3}	1.41×10^{-3}	AFGL
14KaKaTaPe[99]	7911–8104	429/429	1.04×10^{-3}	1.26×10^{-3}	AFGL
53HeHe[100]	8065–8102	24/23	2.33×10^{-2}	7.83×10^{-2}	Other
20KaKaCa[101]	8497–8678	35/35	5.00×10^{-4}	7.84×10^{-4}	AFGL
05DiCaBeTa[102]	8815–9419	271/271	2.27×10^{-3}	5.91×10^{-3}	AFGL
15PeSoSoLy[103]	9253–9419	73/73	5.10×10^{-4}	2.98×10^{-3}	AFGL
05WaPeTaLi[104]	9256–9419	78/78	3.15×10^{-3}	3.62×10^{-3}	AFGL
01WeCa[105]	10,455–10,747	102/102	5.69×10^{-3}	6.22×10^{-3}	AFGL
12LuLiPaLi[106]	12,272–12,462	168/168	3.38×10^{-3}	3.41×10^{-3}	AFGL
99CaBaTeTa[107]	12,311–12,462	62/62	1.08×10^{-2}	2.01×10^{-2}	Other
00TaPeTeLe[58]	13,577–13,734	65/65	7.43×10^{-3}	8.01×10^{-3}	AFGL
14BiDeMaKa[108]	13,597–13,632	10/10	1.00×10^{-2}	1.89×10^{-2}	AFGL

[a]A/V = Available transitions/Validated transitions.
[b]CSU = Average claimed source uncertainty.
[c]MSU = Average MARVEL-suggested source uncertainty.

the same convention as in Reference 46. 179 of these sources were then classified as sources that include experimental CO_2 line positions, of which 66 sources were identified as having experimental $^{13}C^{16}O_2$ line positions. Additional data were acquired through a private communication and a conference proceeding.

Four of the sources identified[33,35,36,44] provide beat-frequency measurements for $^{13}C^{16}O_2$. In this work we do consider the 636 beat frequency measurements of Reference 33, but only by comparing them with the results of our standard MARVEL analysis. Inclusion of these data in a full MARVEL analysis will have to await generalization of the MARVEL algorithm. Reference 44 measured the beat frequencies between the isotopologues $^{12}C^{16}O_2$ and $^{13}C^{16}O_2$ and also provided absolute $^{13}C^{16}O_2$ frequencies. We were able to include the absolute frequencies in our dataset without any further consideration.

Data from four sources[47–50] were excluded from our final dataset. Reasons for their exclusion is given in Section 3.4.

3.2 | Dataset construction

First, we constructed a dataset comprising the most reliable data, that is, self-consistent data which also have low experimental uncertainty. This master dataset included nearly 70% of our gathered data, the remaining 30% included conflicting data, as well, which had to be analyzed carefully, line by line. For this purpose, we developed a code that automates the MARVEL input procedure and detects lines that produce conflicts with the master dataset. Such lines are referred to as "bad lines". A bad line is not necessarily incorrect, it simply shows the lack of self-consistency in the SN assembled, and the problem could be due to errors present in other lines.

Our first attempts to use this code produced over a thousand bad lines. These lines were then carefully analyzed in order to minimize their number. A large portion of the bad lines were due to misassignments, the rest were due to typos, illegal transitions, and possible misidentification of the isotopologue or molecule.

After reducing the number of bad lines to only 36, which were excluded from the final calculations, we began analyzing the uncertainties suggested by MARVEL. At that point, our SN contained floating components that contained around 300 transitions. 44 lines from CDSD-2019[30] were used to link the floating components with the main component, reducing the number of lines in the floating components to less than 100. The remaining floating components are too fragmentary to link to the main network, we would need to include many more semi-empirical lines than was deemed to be reasonable. The lines from CDSD-2019 were given an uncertainty of 0.0005 cm^{-1}.

Our final dataset contains rovibrational transitions collated from sources given in Table 1. Of the 20,754 experimental transitions gathered, only 14,101 are unique. In fact, 10,665 transitions are measured only once, while there are 5 and 32 transitions measured 10 and 9 times, respectively. The principal component of our final SN contains 20,641 transitions, the other transitions form floating components. The experimentally measured transitions involve 6520 states; we were able to determine absolute energies for 6318 of them.

The $^{13}C^{16}O_2$ lines we have gathered cover the region from 579 to 13,735 cm^{-1}. Figure 2 illustrates the distribution of the collected data, using two vertical axes to help appreciate the amount of experimental data acquired compared to HITRAN2020.[51] One can clearly see that most of the empty regions are due to transparency windows, but there is still a need for more accurate experimental data across the spectrum.

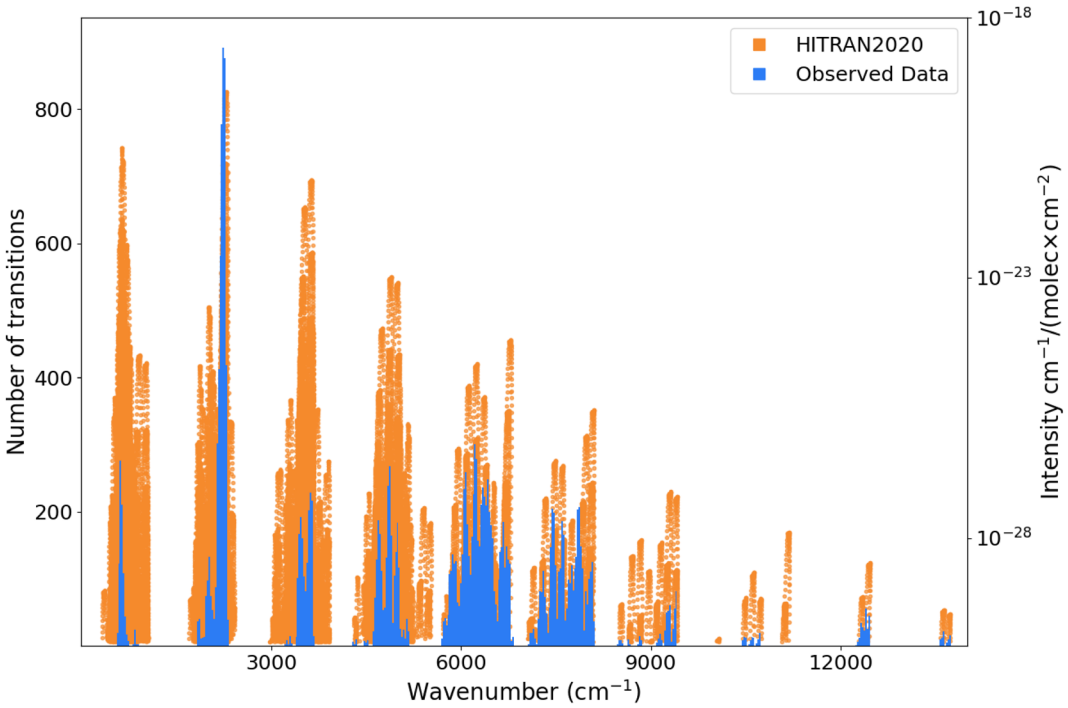

FIGURE 2 Coverage of the transition data obtained from literature sources (see Table 1 for more details). The blue columns follow the left vertical axis, each column covers a region of 25 cm^{-1}. In the background, the spectrum from HITRAN2020[51] is given in orange, with the right vertical axis being the line intensity.

3.3 | Comments on literature sources used

67Hahn:[52] This source provides the same bands twice in two sets of tables, with the second set of tables switching the assigned branch. Our analysis shows that the first table (Table 1) provides the correct branch. No data from other tables were taken.

68ObRaHaMc:[53] Provides two sets of transitions, recorded at two different laboratories. The two datasets were included with distinct tags. Tags 68ObRaHaMcP and 68ObRaHaMcO correspond to datasets from the Pennsylvania and the Ohio laboratories, respectively.

77StToCl:[54] Current theoretical linelists do not provide reliable assignments for the high-energy bands of this source, specifically 004–003, 005–004, 006–005, 007–006, 008–007, 009–008, 014–013, and 015–014, where ℓ_2 is 1 in the latter two cases and zero otherwise. To include these bands in our dataset, AFGL assignments were manually given as: 00041–00031, 00051–00041, 00061–00051, 00071–00061, 00081–00071, 00091–00081, 01141–01131, and 01151–01141, in order. These assignments are based on the assumption that these energy levels are not affected by Fermiresonances, eliminating the complications induced by using older notations. These assignments produced 27 energy levels not present in Ames-2021.[29] Reference 55 was used to verify our assignments.

78BaLiDeRa:[56] This source uses Herzberg's notation. While updating the notation to AFGL, we had to split the 0311e–0310e band into 11112e–11102e and 30001e–11102e. This could be an assignment issue or a result of the difference in notation.

82BaRiSmRa:[57] Uses Herzberg's notation. While updating the notation to AFGL, we had to split the 0311e–0110e band into 11112e–01101e and 30001e–01101e; and split the 3000–0110 band into 11112e–01101e and 30001e–01101e. This could be an assignment issue or a result of the difference in notation.

00TaPeTeLe:[58] Contains two transitions connected to an energy level, 25 2 0 0 5 2 e, not present in Ames-2021.[29] As this level is present in HITRAN2020[51] and the transitions do not break any selection rule, they were included in the final dataset.

04DiMaRoPe:[59] Provides over 4000 lines, but does not specify which of these lines are blended, individual uncertainties are not given either. The Q branch lines were not given a parity. The Pauli principle constraint was used to assign parities to the lines. Additionally, this source contains 91 lines which, according to our analysis, are misassigned, and it correctly assigns nine of the lines we suggest are misassigned in 16BeDeSuBr.[60]

08PeDeLiKa:[31] Provides over 3800 lines, but it specifies neither which lines are blended, nor the uncertainty of individual lines. It contains 41 lines for which we suggest new assignments. Correctly assigns 46 lines that we suggest are misassigned in 04DiMaRoPe.[59]

08PePeCa:[32] Contains two lines which we suggest to reassign and correctly assigns 45 lines misassigned in 04DiMaRoPe,[59] 9 of which were already corrected in 08PeDeLiKa,[31] and also correctly assigns 34 lines misassigned in 08PeDeLiKa.[31]

16BeDeSuBr:[60] Contains 15 lines for which we suggest reassignments.

TABLE 2 Reassignments of lines suggested in this study.

Position	Line[a]	Original band	Suggested band	Source
4695.798536	P(60)e	20012 – 00001	20013 – 00001	16BeDeSuBr[60]
4707.264592	R(28)e	30014 – 10001	30014 – 10002	16BeDeSuBr
4797.361758	P(58)e	30013 – 10001	30013 – 10002	16BeDeSuBr
4801.993159	P(54)e	30013 – 10001	30013 – 10002	16BeDeSuBr
4813.081178	P(44)e	30013 – 10001	30013 – 10002	16BeDeSuBr
4833.195386	P(24)e	30013 – 10001	30013 – 10002	16BeDeSuBr
6315.9293	P(26)f	12222 – 01101	23311 – 01101	04DiMaRoPe[59]
6320.7489	P(21)e	12222 – 01101	23311 – 01101	04DiMaRoPe
6336.397	Q(19)e	23311 – 01101	12222 – 01101	08PePeCa[†32]
6336.397	Q(19)e	23311 – 01101	12222 – 01101	08PeDeLiKa[†31]
6336.8879	Q(23)e	12222 – 01101	23311 – 01101	04DiMaRoPe[59]
6337.2449	Q(19)e	12222 – 01101	23311 – 01101	08PeDeLiKa[†31]
6337.2449	Q(19)e	12222 – 01101	23311 – 01101	04DiMaRoPe[†59]
6351.0222	R(18)f	23311 – 01101	12222 – 01101	08PePeCa[†32]
6351.0222	R(18)f	23311 – 01101	12222 – 01101	08PeDeLiKa[†31]
6351.8689	R(18)f	12222 – 01101	23311 – 01101	08PeDeLiKa[†]
6351.8689	R(18)f	12222 – 01101	23311 – 01101	04DiMaRoPe[†59]
6358.3762	R(28)f	12222 – 01101	23311 – 01101	04DiMaRoPe
6402.7482	R(70)e	30011 – 00001	11122 – 00001	04DiMaRoPe[†]
6402.7482	R(70)e	30011 – 00001	11122 – 00001	08PeDeLiKa[†31]
6452.1822	R(53)f	32211 – 02201	21122 – 02201	08PeDeLiKa[†]
6452.1822	R(53)f	32211 – 02201	21122 – 02201	04DiMaRoPe[†59]
6454.4725	R(47)f	21122 – 02201	32211 – 02201	04DiMaRoPe[†]
6454.4725	R(47)f	21122 – 02201	32211 – 02201	08PeDeLiKa[†31]
6458.3448	R(57)f	21122 – 02201	32211 – 02201	04DiMaRoPe[59]

[a]The *J* value and parity given for the lower state.
[†]These are duplicate lines.

3.4 | Comments on literature sources not used

45NiYa:[47] The claimed uncertainty of this source is 0.07 cm^{-1}. It covers the region 2243–2329 cm^{-1}, which is well covered by other, higher-resolution studies.

66GoMc:[48] The lines provided are identical to those in a previous publication from the same group.[61]

82EsHuVa:[49] The lines provided are identical to those in another publication.[24]

06ZhQuReHu:[50] The data show large discrepancies with other sources. Although it covers the region 912–937 cm^{-1}, which is not covered by any other source, no new energy levels are determined by this source.

4 | RESULTS AND DISCUSSION

4.1 | Relabeling of states

For the sake of unifying the notation of the energy levels across the entire dataset, we had to update the labels of 5149 lines collected from 21 sources, see Table 1. During the update, we found many lines whose assignment disagreed with the rest of the dataset. To check the assignments, these lines were compared to lines present in the Ames-2021[29] line list. We propose corrections for 148 misassigned lines, 18 of which are reported with the updated assignment within experimental accuracy for the first time. These lines are listed in Table 2.

4.2 | Dataset of empirical energy levels

The 14,101 unique rovibrational transitions gathered yielded 6318 empirical rovibrational energy levels for $^{13}C^{16}O_2$. Table A1 in the Appendix summarizes the vibrational bands which could be determined based on the set of measured rovibrational transitions.

Figure 3 illustrates the distribution of the transitions used for the determination of each energy level. As usual, this is a heavy-tailed degree distribution. Figure 4 illustrates the uncertainty distribution of our empirical energy levels. While the overall uncertainty is satisfactory, more high-resolution measurements are needed to eliminate the outliers and to expand the data coverage.

4.3 | Beat frequency comparisons

While we were unable to extend our SN with the available beat-frequency measurements, we were able to compare the originally measured frequencies with frequencies computed using our empirical (MARVEL) energy levels. Table 3 summarizes the results obtained and contains a comparison with the beat frequencies of Reference 33. As seen there, (a) in most cases MARVEL can reproduce the measured frequencies within the MARVEL uncertainties, computed from the uncertainties of the empirical energy levels, and (b) the MARVEL uncertainties are significantly larger than the uncertainties of the beat-frequency measurements. These observations show the importance and the utility of including beat frequency data in a spectroscopic network.

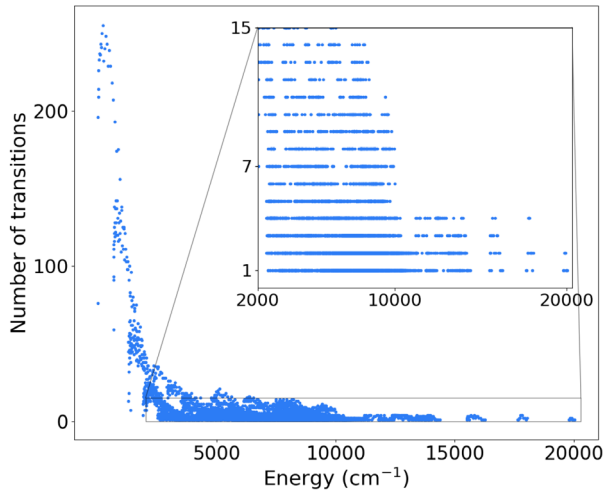

FIGURE 3 Number of transitions used for determining the energies of each state.

4.4 | Comparison with line lists

A comparison of our data with available line lists shows good overall agreement with both the CDSD-2019[30] and the Ames-2021[29] data. It should also be noted that our data show better agreement with CDSD-2019 than with Ames-2021. Figure 5 shows systematic differences between the Ames-2021 and the CDSD-2019 data and illustrates the good agreement between our dataset and CDSD-2019. The outliers highlighted in the figure were determined using only a single transition; we tried to find more experimental data in these regions but none was found. Figure 6 compares the energy-level coverage, as a function of J, between our dataset and that of Ames-2021. Evidently, we need a lot more experimental data for the region above the 10,000 cm^{-1} region.

5 | SUMMARY

This paper describes a comprehensive analysis of the high-resolution, rovibrational spectroscopy literature available for the second most abundant isotopologue of carbon dioxide, $^{13}C^{16}O_2$. All the assigned transitions, altogether from 60 literature sources, have been extracted and verified using appropriate selection rules,

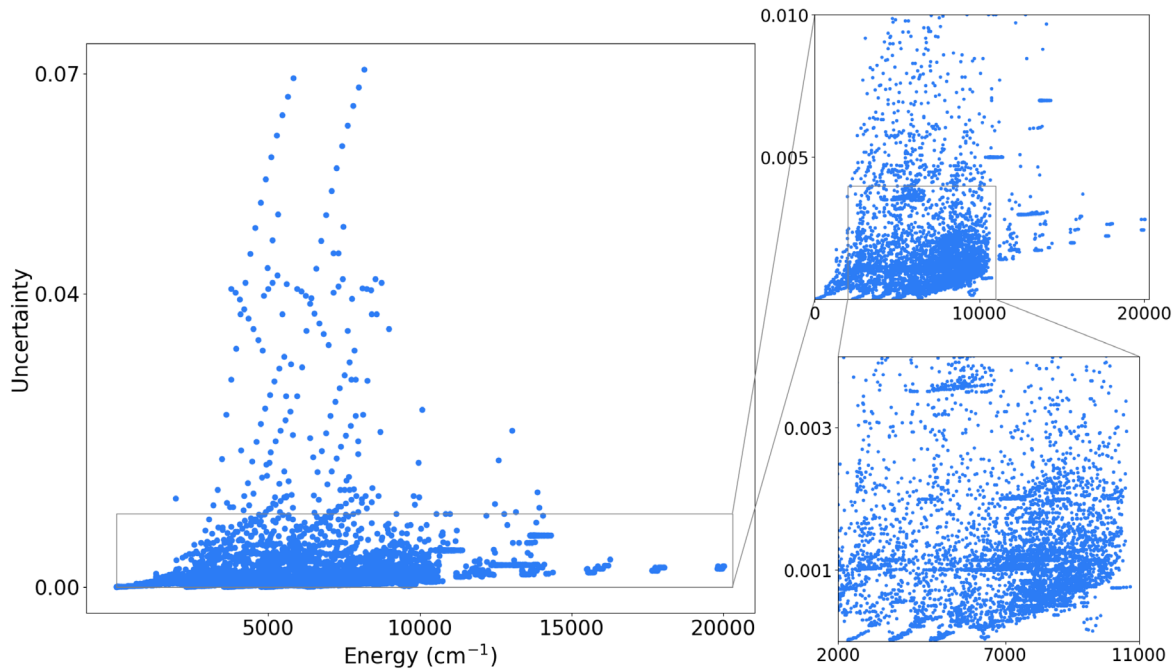

FIGURE 4 Uncertainty distribution of the empirical rovibrational energy levels of this study. Our average uncertainty is 0.0024 cm^{-1}, with 179 outliers having an uncertainty above 0.01 cm^{-1}.

TABLE 3 Comparison of beat-frequency measurements from Reference 33, in MHz, with results of the present study.

Frequency[a]	Unc.	Sequence transition		Reference transition		*MP*[b]	*MU*[c]	$\Delta\nu$[d]
−11,156.4	0.8	P(3)e	00021-10011	P(6)e	00011-10001	−11,148.9	24.2	−7.5
−9905.8	0.8	P(5)e	00021-10011	P(8)e	00011-10001	−9928.1	32.1	22.3
−8649.0	0.8	P(7)e	00021-10011	P(10)e	00011-10001	−8658.0	32.1	9.0
−7387.3	0.8	P(9)e	00021-10011	P(12)e	00011-10001	−7358.8	38.5	−28.5
−6114.2	0.8	P(11)e	00021-10011	P(14)e	00011-10001	−6098.6	26.6	−15.6
−4836.2	0.8	P(13)e	00021-10011	P(16)e	00011-10001	−4826.6	35.8	−9.6
−3548.0	0.8	P(15)e	00021-10011	P(18)e	00011-10001	−3564.2	34.1	16.2
−2252.3	0.8	P(17)e	00021-10011	P(20)e	00011-10001	−2229.6	43.2	−22.7
−948.5	0.8	P(19)e	00021-10011	P(22)e	00011-10001	−925.3	21.8	−23.2
365.0	0.8	P(21)e	00021-10011	P(24)e	00011-10001	367.5	24.0	−2.5
1687.7	0.8	P(23)e	00021-10011	P(26)e	00011-10001	1699.4	24.4	−11.7
3020.2	0.8	P(25)e	00021-10011	P(28)e	00011-10001	3039.4	30.4	−19.2
4360.9	0.8	P(27)e	00021-10011	P(30)e	00011-10001	4379.6	15.3	−18.7
5714.4	0.8	P(29)e	00021-10011	P(32)e	00011-10001	5742.0	20.5	−27.6
7077.1	0.8	P(31)e	00021-10011	P(34)e	00011-10001	7107.3	23.0	−30.2
8446.4	0.8	P(33)e	00021-10011	P(36)e	00011-10001	8473.6	20.3	−27.2
9832.0	0.8	P(35)e	00021-10011	P(38)e	00011-10001	9854.2	26.2	−22.1
11,225.3	0.8	P(37)e	00021-10011	P(40)e	00011-10001	11,257.2	34.1	−31.9
12,631.0	0.8	P(39)e	00021-10011	P(42)e	00011-10001	12,651.3	35.6	−20.3
14,047.5	0.8	P(41)e	00021-10011	P(44)e	00011-10001	14,080.7	29.6	−33.2
15,478.3	0.8	P(43)e	00021-10011	P(46)e	00011-10001	15,521.8	38.1	−43.5
16,921.9	0.8	P(45)e	00021-10011	P(48)e	00011-10001	16,958.9	38.0	−37.0
18,373.0	0.8	P(47)e	00021-10011	P(50)e	00011-10001	18,416.4	48.5	−43.3
−17,907.8	0.8	R(7)e	00021-10011	R(4)e	00011-10001	−17,881.1	40.8	−26.7
−19,117.7	0.8	R(9)e	00021-10011	R(6)e	00011-10001	−19,100.5	26.7	−17.2
−20,317.7	0.8	R(11)e	00021-10011	R(8)e	00011-10001	−20,307.6	34.9	−10.1
−21,515.3	0.8	R(13)e	00021-10011	R(10)e	00011-10001	−21,526.8	32.1	11.5
−22,709.2	0.8	R(15)e	00021-10011	R(12)e	00011-10001	−22,680.0	41.7	−29.2
18,563.3	0.8	R(17)e	00021-10011	R(12)e	00011-10001	18,577.4	19.4	−14.1
16,784.1	0.8	R(19)e	00021-10011	R(14)e	00011-10001	16,792.8	26.6	−8.7
15,010.6	0.8	R(21)e	00021-10011	R(16)e	00011-10001	15,014.1	22.8	−3.5
13,235.2	0.8	R(23)e	00021-10011	R(18)e	00011-10001	13,255.1	30.4	−19.8
11,465.5	0.8	R(25)e	00021-10011	R(20)e	00011-10001	11,477.8	18.8	−12.3
9697.0	0.8	R(27)e	00021-10011	R(22)e	00011-10001	9728.4	18.6	−31.4
7928.1	0.8	R(29)e	00021-10011	R(24)e	00011-10001	7956.4	19.3	−28.3
6157.9	0.8	R(31)e	00021-10011	R(26)e	00011-10001	6177.7	19.2	−19.8
4388.8	0.8	R(33)e	00021-10011	R(28)e	00011-10001	4412.5	24.3	−23.7
2620.3	0.8	R(35)e	00021-10011	R(30)e	00011-10001	2645.9	33.5	−25.6
855.6	0.8	R(37)e	00021-10011	R(32)e	00011-10001	865.1	31.2	−9.5
−917.5	0.8	R(39)e	00021-10011	R(34)e	00011-10001	−890.2	28.8	−27.3
−2685.8	0.8	R(41)e	00021-10011	R(36)e	00011-10001	−2661.8	26.7	−24.0

[a]The beat frequency is given as the frequency of the sequence transition − the frequency of the reference transition.
[b]*MP* = MARVEL predicted frequency.
[c]*MU* = Uncertainty of the MARVEL predicted frequency.
[d]The difference between the measured and the MARVEL-predicted frequency.

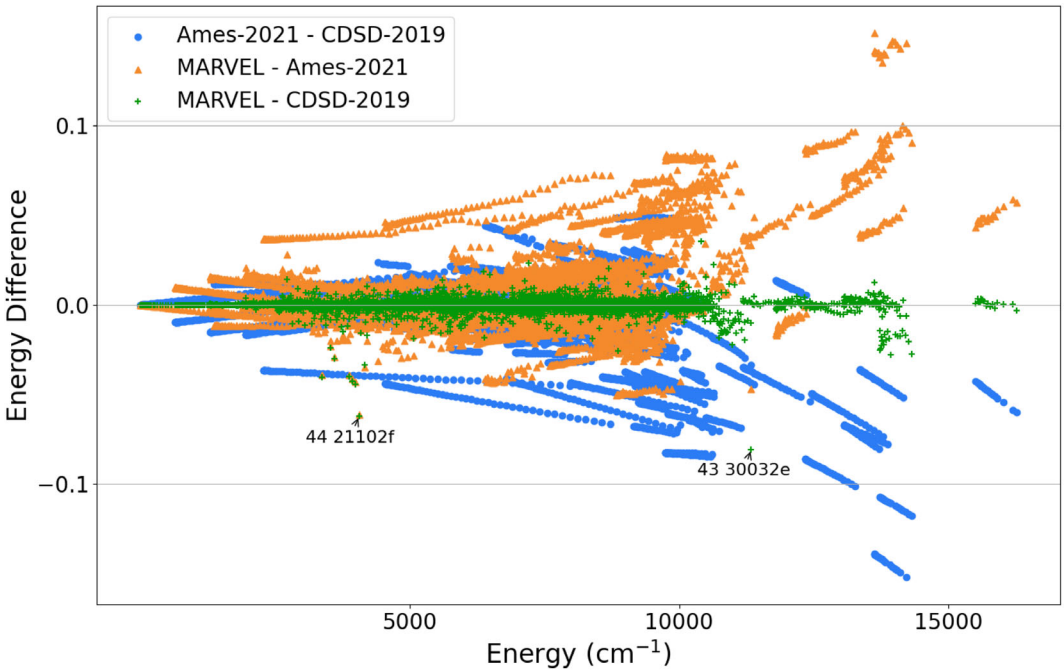

FIGURE 5 Comparison between the MARVEL, Ames-2021,[29] and CDSD-2019[30] rovibrational energies (in cm^{-1}). The average absolute difference between MARVEL and Ames-2021 is 0.0161 cm^{-1}, while the average absolute difference between MARVEL and CDSD-2019 is as small as 0.0016 cm^{-1}. The maximum absolute difference between MARVEL and Ames-2021 is 0.1516 cm^{-1}, while the maximum absolute difference between MARVEL and CDSD-2019 is 0.0806 cm^{-1}.

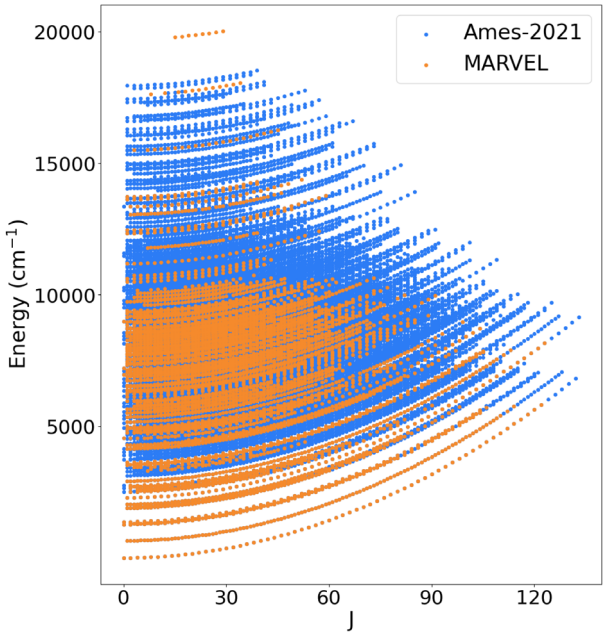

FIGURE 6 Energy-level coverage of our dataset against that of Ames-2021.[29] See Table A1 of the Appendix for more information on specific bands.

the MARVEL algorithm, and a comparative analysis against available line lists. These extensive comparisons were performed to ensure the validity of the labelling of the states involved in the measured transitions. The conventions in use for the labelling of CO_2 lines were briefly reviewed as in several cases a conversion had to be performed.

The validated data cover the wavenumber range 579–13,735 cm^{-1}. Our detailed analysis reveals (a) areas in the spectrum where there is a lack of data, (b) numerous inconsistencies in the vibrational assignment of some of the measured transitions (we report 18 possible errors for the first time), and (c) conflicting labels of higher-energy levels between experimental data[54,58] and theoretical line lists.

A comparison between our energy levels and those of Ames-2021[29] and CDSD-2019[30] shows significantly better agreement with CDSD-2019, highlighting the importance of fitting theoretical models using available experimental data. Further research is being carried out in our groups to analyze more isotopologues of CO_2. Work is also underway to explore methods of including the beat frequency data into the MARVEL analysis procedure; initial attempts to do this show that there are numerical difficulties with ill-conditioned matrices which will need to be overcome before this can be done usefully.

ACKNOWLEDGMENTS

We thank STFC for funding the UK–Jordan collaboration under Newton Fund grant ST/T001429/1. Jonathan Tennyson thanks the European Research Council (ERC) for support under the European Union's Horizon 2020 research and innovation programme through Advance grant number 883830. The work performed in Budapest received funding from the HUN-REN Hungarian Research Network and from the National Research, Development and Innovation Office (NKFIH, grant no. K138233). This publication supports research

performed within the COST Action CA21101 "Confined molecular systems: from a new generation of materials to the stars" (COSY), funded by the European Cooperation in Science and Technology (COST), and the PHYMOL (Physics, Accuracy and Machine Learning: Towards the Next Generation of Molecular Potentials) project, funded mainly under the Horizon Europe scheme.

DATA AVAILABILITY STATEMENT

The data that supports the findings of this study are available in the supplementary material of this article.

REFERENCES

[1] H.-O. Pörtner, D. Roberts, H. Adams, I. Adelekan, C. Adler, R. Adrian, P. Aldunce, E. Ali, R. A. Begum, B. B. Friedl, R. B. Kerr, R. Biesbroek, J. Birkmann, K. Bowen, M. Caretta, J. Carnicer, E. Castellanos, T. Cheong, W. Chow, G. C. G. Cissé, Z. Z. Ibrahim, *Climate Change 2022: Impacts, Adaptation and Vulnerability, Technical Summary*, Cambridge University Press, Cambridge, UK and New York, USA **2022**.

[2] K. P. Shine, G. E. Perry, *Q. J. R. Meteorol.* **2023**, *149*, 1856.

[3] R. A. Toth, L. R. Brown, C. E. Miller, V. M. Devi, D. C. Benner, *J. Quant. Spectrosc. Radiat. Transf.* **2008**, *109*, 906.

[4] C. Abia, J. Isern, *Mon. Not. R. Astron. Soc.* **1997**, *289*, L11.

[5] M. R. Swain, G. Vasisht, G. Tinetti, J. Bouwman, P. Chen, Y. Yung, D. Deming, P. Deroo, *Astrophys. J. Lett.* **2009**, *690*, L114.

[6] E.-M. Ahrer, L. Alderson, N. M. Batalha, N. E. Batalha, J. L. Bean, T. G. Beatty, T. J. Bell, B. Benneke, Z. K. Berta-Thompson, A. L. Carter, I. J. M. Crossfield, N. Espinoza, A. D. Feinstein, J. J. Fortney, N. P. Gibson, J. M. Goyal, E. M.-R. Kempton, J. Kirk, L. Kreidberg, M. Lopez-Morales, M. R. Line, J. D. Lothringer, S. E. Moran, S. Mukherjee, K. Ohno, V. Parmentier, C. Piaulet, Z. Rustamkulov, E. Schlawin, D. K. Sing, K. B. Stevenson, H. R. Wakeford, N. H. Allen, S. M. Birkmann, J. Brande, N. Crouzet, P. E. Cubillos, M. Damiano, J.-M. Desert, P. Gao, J. Harrington, R. Hu, S. Kendrew, H. A. Knutson, P.-O. Lagage, J. Leconte, M. Lendl, R. J. MacDonald, E. M. May, Y. Miguel, K. Molaverdikhani, J. Moses, C. A. Murray, M. Nehring, N. K. Nikolov, D. J. M. P. D. de la Roche, M. Radica, P.-A. Roy, K. G. Stassun, J. Taylor, W. C. Waalkes, P. Wachiraphan, L. Welbanks, P. J. Wheatley, K. Aggarwal, M. K. Alam, A. Banerjee, J. K. Barstow, J. Blecic, S. L. Casewell, Q. Changeat, K. L. Chubb, *Nature* **2023**, *614*, *649*.

[7] Y. Zhang, I. A. G. Snellen, A. J. Bohn, P. Molliere, C. Ginski, H. J. Hoeijmakers, M. A. Kenworthy, E. E. Mamajek, T. Meshkat, M. Reggiani, F. Snik, *Nature* **2021**, *595*, 370.

[8] L. S. Rothman, I. E. Gordon, R. J. Barber, H. Dothe, R. R. Gamache, A. Goldman, V. I. Perevalov, S. A. Tashkun, J. Tennyson, *J. Quant. Spectrosc. Radiat. Transf.* **2010**, *111*, 2139.

[9] S. A. Tashkun, V. I. Perevalov, *J. Quant. Spectrosc. Radiat. Transf.* **2011**, *112*, 1403.

[10] S. N. Yurchenko, T. M. Mellor, R. S. Freedman, J. Tennyson, *Mon. Not. R. Astron. Soc.* **2020**, *496*, 5282.

[11] X. Huang, R. S. Freedman, S. Tashkun, D. W. Schwenke, T. J. Lee, *J. Mol. Spectrosc.* **2023**, *392*, 111748.

[12] A. G. Császár, G. Czakó, T. Furtenbacher, E. Mátyus, *Annu. Rep. Comput. Chem.* **2007**, *3*, 155.

[13] T. Furtenbacher, A. G. Császár, J. Tennyson, *J. Mol. Spectrosc.* **2007**, *245*, 115.

[14] T. Furtenbacher, A. G. Császár, *J. Quant. Spectrosc. Radiat. Transf.* **2012**, *113*, 929.

[15] R. Tóbiás, T. Furtenbacher, J. Tennyson, A. G. Császár, *Phys. Chem. Chem. Phys.* **2019**, *21*, 3473.

[16] A. G. Császár, T. Furtenbacher, *J. Mol. Spectrosc.* **2011**, *266*, 99.

[17] T. Furtenbacher, P. Árendás, G. Mellau, A. G. Császár, *Sci. Rep.* **2014**, *4*, 4654.

[18] A. G. Császár, T. Furtenbacher, P. Árendás, *J. Phys. Chem. A* **2016**, *120*, 8949.

[19] J. Tennyson, S. N. Yurchenko, *Mon. Not. R. Astron. Soc.* **2012**, *425*, 21.

[20] J. Tennyson, S. N. Yurchenko, A. F. Al-Refaie, V. H. J. Clark, K. L. Chubb, E. K. Conway, A. Dewan, M. N. Gorman, C. Hill, A. E. Lynas-Gray, T. Mellor, L. K. McKemmish, A. Owens, O. L. Polyansky, M. Semenov, W. Somogyi, G. Tinetti, A. Upadhyay, I. Waldmann, Y. Wang, S. Wright, O. P. Yurchenko, *J. Quant. Spectrosc. Radiat. Transf.* **2020**, *255*, 107228.

[21] A. R. Al-Derzi, S. N. Yurchenko, J. Tennyson, M. Melosso, N. Jiang, C. Puzzarini, L. Dore, T. Furtenbacher, R. Tóbiás, A. G. Császár, *J. Quant. Spectrosc. Radiat. Transf.* **2021**, *266*, 107563.

[22] G. Ecseri, I. Simkó, T. Furtenbacher, B. Rácsai, L. Fusina, G. Di Lonardo, K. A. Peterson, A. G. Császár, *J. Mol. Spectrosc.* **2023**, *397*, 111834.

[23] R. A. McClatchey, W. S. Benedict, S. A. Clough, D. E. Burch, R. F. Calfee, K. Fox, L. S. Rothman, J. S. Garing, AFCRL atmospheric absorption line parameters compilation. Tech. Rep. AFCRL-TR-73-0096, Air Force Cambridge Research Laboratories **1983** https://modis-images.gsfc.nasa.gov/JavaHAWKS/AFCRL˙AALPC.pdf

[24] M. P. Esplin, R. J. Huppi, H. Sakai, G. A. Vanasse, L. S. Rothman, Absorption measurements of CO_2 and H_2O at high resolution and elevated temperatures. Tech. Rep. AFGL-TR-82-0057, Utah State University **1982** https://apps.dtic.mil/sti/citations/ADA113824

[25] B. Perevalov, Le spectre d'absorption du dioxyde de carbone dans le proche infrarouge (1.4-1.7 μm): Cavity Ring Down Spectroscopy, modélisation globale et bases de données. Theses, Université Joseph-Fourier–Grenoble I **2009** https://theses.hal.science/tel-00600074

[26] G. Amat, M. Pimbert, *J. Mol. Spectrosc.* **1965**, *16*, 278.

[27] J. M. Brown, J. T. Hougen, K. P. Huber, J. W. C. Johns, I. Kopp, H. Lefebvre-Brion, A. J. Merer, D. A. Ramsay, J. Rostas, R. N. Zare, *J. Mol. Spectrosc.* **1975**, *55*, 500.

[28] W. D. Allen, Y. Yamaguchi, A. G. Császár, D. A. Clabo Jr., R. B. Remington, H. F. Schaefer III, *Chem. Phys.* **1990**, *145*, 427.

[29] X. Huang, D. W. Schwenke, R. S. Freedman, T. J. Lee, *J. Phys. Chem.* **2022**, *A 126*, 5940.

[30] S. A. Tashkun, V. I. Perevalov, R. R. Gamache, J. Lamouroux, *J. Quant. Spectrosc. Radiat. Transf.* **2019**, *228*, 124.

[31] B. V. Perevalov, T. Deleporte, A. W. Liu, S. Kassi, A. Campargue, J. V. Auwera, S. A. Tashkun, V. I. Perevalov, *J. Quant. Spectrosc. Radiat. Transf.* **2008**, *109*, 2009.

[32] B. V. Perevalov, V. I. Perevalov, A. Campargue, *J. Quant. Spectrosc. Radiat. Transf.* **2008**, *109*, 2437.

[33] K. J. Siemsen, *Opt. Commun.* **1980**, *34*, 447.

[34] K. J. Siemsen, *Opt. Lett.* **1981**, *6*, 114.

[35] A. G. Maki, C. C. Chou, K. M. Evenson, L. R. Zink, J. T. Shy, *J. Mol. Spectrosc.* **1994**, *167*, 211.

[36] L. Bradley, K. Soohoo, C. Freed, *IEEE J. Quantum Electron.* **1986**, *22*, 234.

[37] C. C. Chou, A. G. Maki, S. J. Tochitsky, J. T. Shy, K. M. Evenson, L. R. Zink, *J. Mol. Spectrosc.* **1995**, *172*, 233.

[38] F. R. Petersen, J. S. Wells, K. J. Siemsen, A. M. Robinson, A. G. Maki, *J. Mol. Spectrosc.* **1984**, *105*, 324.

[39] B. G. Whitford, K. J. Siemsen, J. Reid, *Opt. Commun.* **1977**, *22*, 261.

[40] K. J. Siemens, B. G. Whitford, *Opt. Commun.* **1977**, *22*, 11.

[41] V. Bernard, G. Nogues, C. Daussy, L. Constantin, C. Chardonnet, *Metrologia* **1997**, *34*, 313.

[42] J. P. Aldridge, R. F. Holland, H. Flicker, K. W. Nill, T. C. Harman, *J. Mol. Spectrosc.* **1975**, *54*, 328.

[43] C. Freed, A. H. M. Ross, R. G. O'Donnell, *J. Mol. Spectrosc.* **1974**, *49*, 439.

[44] F. R. Petersen, J. S. Wells, A. G. Maki, K. J. Siemsen, *Appl. Opt.* **1981**, *20*, 3635.
[45] J. Tennyson, T. Furtenbacher, S. N. Yurchenko, A. G. Császár, *J. Quant. Spectrosc. Radiat. Transf.* **2024**. (In press)
[46] J. Tennyson, P. F. Bernath, L. R. Brown, A. Campargue, M. R. Carleer, A. G. Császár, R. R. Gamache, J. T. Hodges, A. Jenouvrier, O. V. Naumenko, O. L. Polyansky, L. S. Rothman, R. A. Toth, A. C. Vandaele, N. F. Zobov, L. Daumont, A. Z. Fazliev, T. Furtenbacher, I. E. Gordon, S. N. Mikhailenko, S. V. Shirin, *J. Quant. Spectrosc. Radiat. Transf.* **2009**, *110*, 573.
[47] A. H. Nielsen, Y. T. Yao, *Phys. Rev.* **1945**, *68*, 173.
[48] H. R. Gordon, T. K. McCubbin, *J. Mol. Spectrosc.* **1966**, *19*, 137.
[49] M. P. Esplin, R. J. Huppi, G. A. Vanasse, *Appl. Opt.* **1982**, *21*, 1681.
[50] L.-l. Zhang, Y.-C. Qu, D.-M. Ren, X.-Y. Hu, in *Atomic and Molecular Pulsed Lasers VI*, Vol. 6263 (Eds: V. F. Tarasenko, G. Mayer, G. G. Petrash), International Society for Optics and Photonics, SPIE, Tomsk, Russia **2006**, 62630U. https://doi.org/10.1117/12.677448
[51] I. E. Gordon, L. S. Rothman, R. J. Hargreaves, R. Hashemi, E. V. Karlovets, F. M. Skinner, E. K. Conway, C. Hill, R. V. Kochanov, Y. Tan, P. Wcisło, A. A. Finenko, K. Nelson, P. F. Bernath, M. Birk, V. Boudon, A. Campargue, K. V. Chance, A. Coustenis, B. J. Drouin, J. M. Flaud, R. R. Gamache, J. T. Hodges, D. Jacquemart, E. J. Mlawer, A. V. Nikitin, V. I. Perevalov, M. Rotger, J. Tennyson, G. C. Toon, H. Tran, V. G. Tyuterev, E. M. Adkins, A. Baker, A. Barbe, E. Canè, A. G. Császár, A. Dudaryonok, O. Egorov, A. J. Fleisher, H. Fleurbaey, A. Foltynowicz, T. Furtenbacher, J. J. Harrison, J. M. Hartmann, V. M. Horneman, X. Huang, T. Karman, J. Karns, S. Kassi, I. Kleiner, V. Kofman, F. Kwabia-Tchana, N. N. Lavrentieva, T. J. Lee, D. A. Long, A. A. Lukashevskaya, O. M. Lyulin, V. Y. Makhnev, W. Matt, S. T. Massie, M. Melosso, S. N. Mikhailenko, D. Mondelain, H. S. P. Müller, O. V. Naumenko, A. Perrin, O. L. Polyansky, E. Raddaoui, P. L. Raston, Z. D. Reed, M. Rey, C. Richard, R. Tóbiás, *J. Quant. Spectrosc. Radiat. Transf.* **2022**, *277*, 107949.
[52] Y. H. Hahn, The absorption and emission spectra of carbon-dioxide at 4.3 microns. Ph.D. thesis, The Pennsylvania State University **1967** https://www.proquest.com/openview/074bf2696a7b47d2793ca1d620a02193/1?pq-origsite=gscholar&cbl=18750&diss=y
[53] R. Oberly, K. N. Rao, Y. H. Hahn, T. K. McCubbin, *J. Mol. Spectrosc.* **1968**, *25*, 138.
[54] D. A. Steiner, T. R. Todd, C. M. Clayton, T. K. McCubbin, S. R. Polo, *J. Mol. Spectrosc.* **1977**, *64*, 438.
[55] L. S. Rothman, R. L. Hawkins, R. B. Wattson, R. R. Gamache, *J. Quant. Spectrosc. Radiat. Transf.* **1992**, *48*, 537.
[56] A. Baldacci, L. Linden, V. M. Devi, K. N. Rao, B. Fridovich, *J. Mol. Spectrosc.* **1978**, *72*, 135.
[57] A. Baldacci, C. P. Rinsland, M. A. H. Smith, K. N. Rao, *J. Mol. Spectrosc.* **1982**, *94*, 351.
[58] S. A. Tashkun, V. I. Perevalov, J. L. Teffo, M. Lecoutre, T. R. Huet, A. Campargue, D. Bailly, M. P. Esplin, *J. Mol. Spectrosc.* **2000**, *200*, 162.
[59] Y. Ding, P. Macko, D. Romanini, V. Perevalov, S. Tashkun, J.-L. Teffo, S.-M. Hu, A. Campargue, *J. Mol. Spectrosc.* **2004**, *226*, 146.
[60] D. C. Benner, V. M. Devi, K. Sung, L. R. Brown, C. E. Miller, V. H. Payne, B. J. Drouin, S. Yu, T. J. Crawford, A. W. Mantz, M. A. H. Smith, R. R. Gamache, *J. Mol. Spectrosc.* **2016**, *326*, 21.
[61] H. R. Gordon, The infrared spectrum of CO_2 in the 2.8 and 15 micron regions. Ph.D. thesis, The Pennsylvania State University **1965** https://www.proquest.com/openview/59dcaa567b3cb6b908786d3699a70cc9/1?pq-origsite=gscholar&cbl=18750&diss=y
[62] K. Jolma, *J. Mol. Spectrosc.* **1985**, *111*, 211.
[63] R. Paso, J. Kauppinen, R. Anttila, *J. Mol. Spectrosc.* **1980**, *79*, 236.
[64] C. E. Miller, Private communication. **2023**.
[65] K. Jolma, J. Kauppinen, V. M. Horneman, *J. Mol. Spectrosc.* **1983**, *101*, 300.
[66] G. Guelachvili, K. R. Rao, *Handbook of Infrared Standards*, Academic Press, Florida **1986**.
[67] M. J. Reisfeld, M. Flicker, *J. Mol. Spectrosc.* **1978**, *69*, 330.
[68] C. P. Rinsland, D. C. Benner, V. M. Devi, P. S. Ferry, C. H. Sutton, D. J. Richardson, *Appl. Opt.* **1984**, *23*, 2051.
[69] C. P. Rinsland, D. C. Benner, V. M. Devi, *Appl. Opt.* **1985**, *24*, 1644.
[70] C. P. Rinsland, D. C. Benner, *Appl. Opt.* **1984**, *23*, 4523.
[71] O. M. Lyulin, E. V. Karlovets, D. Jacquemart, Y. Lu, A. W. Liu, V. I. Perevalov, *J. Quant. Spectrosc. Radiat. Transf.* **2012**, *113*, 2167.
[72] C. P. Rinsland, D. C. Benner, V. M. Devi, *Appl. Opt.* **1986**, *25*, 1204.
[73] M. P. Esplin, H. Sakai, L. S. Rothman, G. A. Vanasse, W. M. Barowy, R. J. Huppi, Carbon dioxide line positions in the 2.8 and 4.3 micron regions at 800 Kelvin. Tech. Rep. AFGL-TR-86-0046, Utah State University **1986**. https://apps.dtic.mil/sti/citations/ADA173808
[74] M. P. Esplin, L. S. Rothman, *J. Mol. Spectrosc.* **1986**, *116*, 351.
[75] M. P. Esplin, L. S. Rothman, *J. Mol. Spectrosc.* **1983**, *100*, 193.
[76] V. M. Devi, A. Baldacci, J. Grangaard, L. Linden, K. N. Rao, B. Fridovich, *J. Mol. Spectrosc.* **1978**, *70*, 160.
[77] D. Bailly, C. Rossetti, *J. Mol. Spectrosc.* **1984**, *105*, 229.
[78] B. M. Elliott, K. Sung, C. E. Miller, *J. Mol. Spectrosc.* **2015**, *312*, 78.
[79] G. Guelachvili, *J. Mol. Spectrosc.* **1980**, *79*, 72.
[80] D. C. Benner, V. M. Devi, C. P. Rinsland, P. S. Ferry-Leeper, *Appl. Opt.* **1988**, *27*, 1588.
[81] Y. G. Borkov, D. Jacquemart, O. M. Lyulin, S. A. Tashkun, V. I. Perevalov, *J. Quant. Spectrosc. Radiat. Transf.* **2014**, *137*, 57.
[82] W. L. France, F. P. Dickey, *J. Chem. Phys.* **2004**, *23*, 471.
[83] S. Vasilchenko, M. Konefal, D. Mondelain, S. Kassi, P. Čermák, S. A. Tashkun, V. I. Perevalov, A. Campargue, *J. Quant. Spectrosc. Radiat. Transf.* **2016**, *184*, 233.
[84] A. Garnache, A. Liu, L. Cerutti, A. Campargue, *Chem. Phys. Lett.* **2005**, *416*, 22.
[85] A. A. Marinina, Y. G. Borkov, T. M. Petrova, A. M. Solodov, A. A. Solodov, V. I. Perevalov, *Atmos. Ocean. Opt.* **2022**, *35*, 8.
[86] Y. G. Borkov, D. Jacquemart, O. M. Lyulin, S. A. Tashkun, V. I. Perevalov, *J. Quant. Spectrosc. Radiat. Transf.* **2015**, *159*, 1.
[87] L. Goldberg, O. C. Mohler, R. R. Mcmath, A. K. Pierce, *Phys. Rev.* **1949**, *76*, 1848.
[88] L. E. Christensen, G. D. Spiers, R. T. Menzies, J. C. Jacob, *J. Quant. Spectrosc. Radiat. Transf.* **2012**, *113*, 739.
[89] E. V. Karlovets, A. D. Sidorenko, P. Čermák, D. Mondelain, S. Kassi, V. I. Perevalov, A. Campargue, *J. Mol. Spectrosc.* **2018**, *354*, 54.
[90] P. Čermák, E. V. Karlovets, D. Mondelain, S. Kassi, V. I. Perevalov, A. Campargue, *J. Quant. Spectrosc. Radiat. Transf.* **2018**, *207*, 95.
[91] B. V. Perevalov, S. Kassi, D. Romanini, V. I. Perevalov, S. A. Tashkun, A. Campargue, *J. Mol. Spectrosc.* **2006**, *238*, 241.
[92] V. M. Devi, D. C. Benner, K. Sung, L. R. Brown, T. J. Crawford, C. E. Miller, B. J. Drouin, V. H. Payne, S. Yu, M. A. H. Smith, A. W. Mantz, R. R. Gamache, *J. Quant. Spectrosc. Radiat. Transf.* **2016**, *177*, 117.
[93] B. V. Perevalov, S. Kassi, D. Romanini, V. I. Perevalov, S. A. Tashkun, A. Campargue, *J. Mol. Spectrosc.* **2007**, *241*, 90.
[94] A. W. Liu, F. H. Cao, Z. T. Zhang, S. M. Hu, Precision spectroscopy of extremely weak transitions, Paper presented at: The Twenty-eighth Colloquium on High Resolution Molecular Spectroscopy, Dijon, **2023**.
[95] A. Campargue, K. F. Song, N. Mouton, V. I. Perevalov, S. Kassi, *J. Quant. Spectrosc. Radiat. Transf.* **2010**, *111*, 659.
[96] S. Kassi, K. F. Song, A. Campargue, *J. Quant. Spectrosc. Radiat. Transf.* **2009**, *110*, 1801.
[97] K. F. Song, S. Kassi, S. A. Tashkun, V. I. Perevalov, A. Campargue, *J. Quant. Spectrosc. Radiat. Transf.* **2010**, *111*, 332.
[98] S. Kassi, E. V. Karlovets, S. A. Tashkun, V. I. Perevalov, A. Campargue, *J. Quant. Spectrosc. Radiat. Transf.* **2017**, *187*, 414.
[99] E. V. Karlovets, S. Kassi, S. A. Tashkun, V. I. Perevalov, A. Campargue, *J. Quant. Spectrosc. Radiat. Transf.* **2014**, *144*, 137.
[100] G. Herzberg, L. Herzberg, *J. Opt. Soc. Am.* **1953**, *43*, 1037.
[101] E. V. Karlovets, S. Kassi, A. Campargue, *J. Quant. Spectrosc. Radiat. Transf.* **2020**, *247*, 106942.

[102] Y. Ding, A. Campargue, E. Bertseva, S. Tashkun, V. I. Perevalov, *J. Mol. Spectrosc.* **2005**, *231*, 117.
[103] T. M. Petrova, A. M. Solodov, A. A. Solodov, O. M. Lyulin, Y. G. Borkov, S. A. Tashkun, V. I. Perevalov, *J. Quant. Spectrosc. Radiat. Transf.* **2015**, *164*, 109.
[104] L. Wang, V. I. Perevalov, S. A. Tashkun, A. W. Liu, S. M. Hu, *J. Mol. Spectrosc.* **2005**, *233*, 297.
[105] G. Weirauch, A. Campargue, *J. Mol. Spectrosc.* **2001**, *207*, 263.
[106] Y. Lu, A. W. Liu, H. Pan, X. F. Li, V. I. Perevalov, S. A. Tashkun, S.-M. Hu, *J. Quant. Spectrosc. Radiat. Transf.* **2012**, *113*, 2197.
[107] A. Campargue, D. Bailly, J. L. Teffo, S. A. Tashkun, V. I. Perevalov, *J. Mol. Spectrosc.* **1999**, *193*, 204.
[108] A. Bierret, Q. Desbois, J.-L. Martin, S. Kassi, S. A. Tashkun, V. I. Perevalov, A. Campargue, *J. Mol. Spectrosc.* **2014**, *298*, 38.

SUPPORTING INFORMATION

Additional supporting information can be found online in the Supporting Information section at the end of this article.

How to cite this article: M. T. I. Ibrahim, D. Alatoom, T. Furtenbacher, A. G. Császár, S. N. Yurchenko, A. A. A. Azzam, J. Tennyson, *J. Comput. Chem.* **2024**, 1. https://doi.org/10.1002/jcc.27266

APPENDIX

TABLE A1 Vibrational bands of $^{13}C^{16}O_2$.

Band	*LE*[a]	*NE*[b]	Range of *J*	Band	*LE*[a]	*NE*[b]	Range of *J*
00001e	0.0(0)	62	0–122	32214e	7163.9262(8)	25	3–53
01101e	649.2595(2)	55	1–109	04421e	7178.2085(3)	14	18–44
01101f	650.8258(4)	57	2–114	20021e	7209.179(1)	31	0–60
10002e	1265.8277(6)	53	0–104	51104e	7243.8184(9)	19	15–51
02201e	1299.6152(8)	49	2–106	34401e	7250.593(1)	4	30–36
02201f	1301.9634(8)	46	3–103	34401f	7274.901(1)	4	31–39
10001e	1370.0620(9)	53	0–104	40014e	7332.9823(3)	35	1–71
11102e	1897.319(1)	30	1–59	32213f	7362.027(1)	29	2–58
11102f	1898.8903(10)	38	2–76	32213e	7364.361(1)	28	3–57
03301e	1951.063(4)	43	3–95	01131f	7394.356(1)	38	1–75
03301f	1954.1962(10)	40	4–98	01131e	7395.882(1)	39	2–82
11101e	2037.874(1)	42	1–83	51103e	7409.7282(7)	16	15–55
11101f	2039.4389(8)	38	2–80	40013e	7482.3457(5)	37	1–75
00011e	2284.261645(3)	62	1–123	51102e	7491.4420(8)	32	3–65
20003e	2509.874(1)	36	2–80	32212f	7542.849(1)	32	2–64
12202f	2543.438(2)	20	5–45	32212e	7545.175(1)	29	3–65
12202e	2548.141(1)	18	6–44	21123f	7565.6256(7)	20	2–40
04401e	2603.589(3)	27	4–90	21123e	7567.931(1)	20	3–45
04401f	2607.517(1)	23	5–55	40012e	7600.8927(4)	36	1–73
20002e	2647.401(1)	34	2–80	13322f	7618.004(1)	4	6–22
12201e	2702.611(3)	32	2–64	13322e	7636.5848(7)	7	9–25
12201f	2704.958(1)	34	3–79	51101e	7717.3752(6)	20	9–51
20001e	2752.933(1)	27	2–54	32211f	7722.4531(9)	29	2–58
01111f	2921.0154(5)	57	1–113	32211e	7724.778(1)	28	3–61
01111e	2922.5648(2)	54	2–108	21122e	7727.7224(8)	32	1–63
21102e	3311.539(1)	23	7–53	21122f	7729.2660(6)	23	2–54
21102f	3371.802(1)	7	14–44	41115f	7738.188(1)	19	1–37
13301f	3389.614(1)	9	8–34	41115e	7739.740(1)	18	2–44
13301e	3413.120(1)	5	11–37	40011e	7749.8573(6)	36	1–71
21101e	3438.443(1)	15	3–41	33314f	7774.066(1)	18	3–39
21101f	3441.584(1)	4	4–32	33314e	7785.795(2)	16	6–40
10012e	3528.5139(1)	52	1–105	13321e	7796.191(1)	20	3–43
02211f	3559.649(1)	47	2–104	13321f	7799.280(1)	20	4–44
02211e	3561.9795(6)	48	3–105	21121e	7868.5992(6)	29	1–63
10011e	3633.68371(3)	52	1–103	21121f	7870.1408(4)	28	2–60
11112f	4148.010(4)	38	1–75	15511e	7876.724(1)	1	50–50
11112e	4149.564(4)	36	2–72	41114f	7939.8873(7)	29	1–57
03311f	4199.378(2)	40	3–97	41114e	7941.4353(5)	28	2–56
03311e	4202.499(5)	40	4–94	10032e	7981.945(1)	39	1–77
30001e	4206.782(4)	18	12–50	33313e	8002.237(2)	13	6–34
11111f	4288.475(1)	40	1–81	02231f	8009.633(1)	33	2–66
11111e	4290.0213(3)	41	2–82	02231e	8011.928(1)	35	3–71
31104f	4405.447(2)	1	12–12	33313f	8020.957(1)	15	9–41
31104e	4492.891(2)	11	19–39	10031e	8089.782(1)	36	1–73

TABLE A1 (Continued)

Band	*LE*[a]	*NE*[b]	Range of *J*	Band	*LE*[a]	*NE*[b]	Range of *J*
00021e	4543.550(1)	53	0–104	41113f	8112.1577(7)	30	1–59
31103e	4549.1263(3)	18	7–49	41113e	8113.6989(6)	28	2–58
31102e	4704.931(1)	22	7–49	33312f	8192.652(5)	19	3–47
20013e	4748.83708(3)	38	1–79	33312e	8204.319(2)	18	6–46
12212e	4775.651(6)	29	3–59	41112f	8268.3841(6)	30	1–59
12212f	4778.759(7)	27	4–56	41112e	8269.9250(7)	28	2–56
04411f	4840.208(2)	24	4–54	30023e	8333.327(2)	19	6–44
04411e	4854.254(1)	26	7–91	22222e	8352.8655(7)	19	2–38
20012e	4888.158316(6)	40	1–79	22222f	8355.1786(8)	21	3–43
12211f	4941.166(2)	35	2–78	15511f	8356.452(1)	1	61–61
12211e	4943.493(3)	31	3–63	33311f	8393.883(3)	18	3–43
20011e	4992.1243(2)	39	1–77	33311e	8397.00(1)	18	4–38
01121e	5169.369(1)	47	1–99	41111f	8439.9659(8)	28	1–55
01121f	5170.911(1)	42	2–86	41111e	8441.4986(5)	27	2–54
21113f	5357.785(1)	30	1–61	30022e	8448.575(2)	16	4–50
21113e	5359.336(4)	29	2–58	22221f	8524.1457(8)	18	3–43
13312f	5448.714(4)	17	11–43	50015e	8530.4496(9)	23	1–45
13312e	5458.073(4)	15	12–42	22221e	8547.258(1)	16	8–40
21112f	5520.696(3)	31	1–61	42214f	8560.225(1)	16	4–34
21112e	5522.245(8)	31	2–64	42214e	8564.121(1)	16	5–41
13311f	5609.807(4)	19	7–53	30021e	8574.748(2)	9	6–28
13311e	5630.831(4)	20	10–52	11132f	8579.153(1)	37	1–73
21111f	5663.0342(5)	32	1–63	11132e	8580.681(1)	34	2–68
21111e	5664.581(1)	32	2–66	03331f	8626.042(5)	25	3–51
41104e	5755.245(1)	29	3–61	03331e	8629.104(4)	27	4–58
41104f	5767.046(1)	11	6–36	33301e	8674.459(2)	1	79–79
10022e	5782.358(1)	16	6–36	50014e	8708.0391(7)	25	3–53
02221e	5801.712(1)	26	4–60	11131f	8720.153(1)	29	1–59
02221f	5805.5644(8)	28	5–71	11131e	8721.681(1)	29	2–60
10021e	5880.227(4)	20	4–42	42213f	8747.8884(10)	19	2–44
41103e	5934.4012(2)	26	5–57	42213e	8757.2092(8)	20	5–47
30014e	5952.381(1)	38	1–77	50013e	8836.3328(7)	27	1–55
22213e	5975.618(1)	31	3–65	42212e	8933.2445(9)	20	3–41
22213f	5978.739(1)	20	4–42	42212f	8936.349(1)	19	4–40
41103f	5983.6934(2)	4	12–20	50012e	8970.8269(7)	20	1–41
30013e	6120.3955(2)	44	1–89	00041e	8993.510(1)	32	0–62
41102e	6132.396(1)	6	11–35	42211f	9129.098(1)	14	4–30
22212e	6226.122(1)	27	13–69	42211e	9133.005(1)	16	5–37
30012e	6242.73997(9)	42	1–85	50011e	9149.6947(8)	21	3–49
41101e	6261.692(1)	35	3–73	20033e	9159.6376(8)	30	1–61
22211f	6328.367(1)	26	2–52	12232f	9181.7870(10)	27	2–56
22211e	6330.697(1)	31	3–63	12232e	9184.0881(8)	28	3–59
30011e	6364.3946(9)	42	1–83	04431f	9243.571(2)	14	4–36
11122e	6375.273(1)	38	1–75	04431e	9247.414(2)	14	5–35
11122f	6376.820(1)	28	2–66	20032e	9302.898(2)	27	1–53
42204e	6391.615(1)	9	6–36	51114f	9329.999(1)	11	5–31

(Continues)

TABLE A1 (Continued)

Band	*LE*[a]	*NE*[b]	Range of *J*	Band	*LE*[a]	*NE*[b]	Range of *J*
42204f	6426.900(1)	12	11–47	51114e	9334.7545(5)	3	6–10
11121e	6515.888(1)	38	1–75	12231f	9348.857(1)	19	2–38
11121f	6517.430(1)	33	2–72	12231e	9358.03(1)	19	5–41
31114f	6553.7056(10)	33	1–65	20031e	9404.886(2)	28	1–55
31114e	6555.2570(3)	32	2–64	01141f	9611.182(1)	21	6–46
42203f	6604.2618(4)	20	9–53	01141e	9616.465(2)	20	7–47
42203e	6612.075(1)	20	10–48	21133f	9746.998(1)	23	1–47
14411e	6673.179(1)	6	33–45	21133e	9748.526(2)	23	2–46
31113f	6737.470(1)	36	1–77	13332e	9790.604(4)	18	4–38
31113e	6739.017(1)	35	2–72	13332f	9794.444(1)	19	5–41
50003e	6760.715(1)	8	16–48	21132f	9915.392(4)	21	3–43
00031e	6780.9742(9)	46	1–91	21132e	9918.426(2)	16	4–34
42202e	6797.468(1)	21	10–58	21131e	10058.159(2)	14	4–30
42202f	6806.056(1)	21	11–59	21131f	10061.99(2)	15	5–33
50005e	6816.839(1)	8	34–52	10042e	10180.3674(8)	14	4–38
50002e	6837.173(2)	19	10–54	30033e	10492.208(7)	20	1–41
31112f	6892.826(1)	37	1–77	30032e	10617.579(5)	21	1–43
31112e	6894.368(1)	36	2–76	30031e	10735.547(5)	20	3–41
20023e	6965.147(2)	25	0–48	00051e	11184.232(2)	28	1–57
12222e	6989.223(4)	23	2–46	01151f	11794.690(4)	16	7–39
12222f	6991.543(1)	21	3–51	01151e	11800.676(2)	14	8–38
50001e	7002.735(1)	21	8–52	10052e	12341.784(3)	25	1–49
42201f	7002.850(2)	19	11–59	10051e	12453.345(3)	30	1–59
42201e	7012.223(2)	20	12–54	11151e	13060.919(3)	20	2–46
23311f	7020.891(1)	11	9–31	11151f	13063.184(3)	20	3–41
23311e	7046.5030(4)	9	12–30	00061e	13352.404(2)	25	2–52
31111f	7046.805(1)	36	1–71	20052e	13624.652(7)	19	1–39
31111e	7048.348(1)	34	2–70	20051e	13726.351(7)	19	1–39
20022e	7108.7059(5)	27	2–56	00071e	15498.060(2)	21	3–45
40015e	7142.9410(5)	27	1–53	00081e	17640.311(2)	12	8–34
12221e	7156.568(1)	30	2–60	00091e	19798.365(2)	8	15–29
12221f	7158.880(1)	29	3–59				
32214f	7161.5776(10)	25	2–50				

[a]*LE* = lowest energy-level value within the *J* range with uncertainties in parentheses.
[b]*NE* = Number of energy levels.